Role of rotational-energy defect in collisional transfer between the $5\,^2P_{1/2,3/2}$ levels in rubidium

Matthew D. Rotondaro* and Glen P. Perram
Department of Engineering Physics, Air Force Institute of Technology, Wright-Patterson Air Force Base, Ohio 45433-7765
(Received 1 August 1997)

Steady-state laser-induced fluorescence techniques have been used to study the rates for energy transfer between the $5\,^2P_{1/2,3/2}$ levels in rubidium. The cross sections for collisions with the molecular species H_2, D_2, N_2, CH_4, and CF_4 have been measured as $\sigma_2(^2P_{1/2}\rightarrow{}^2P_{3/2})=10.0$, 21.4, 13.2, 29.5, and 9.5×10^{-16} cm^2 and $\sigma_1(^2P_{3/2}\rightarrow{}^2P_{1/2})=13.9$, 29.8, 18.4, 41.0, and 13.2×10^{-16} cm^2, respectively. Correlation of these spin-orbit transfer probabilities with rotational-energy defect is demonstrated. [S1050-2947(98)02405-6]

PACS number(s): 34.30.+h

I. INTRODUCTION

The collisional transfer of energy between the spin-orbit split ^2P_J levels of the alkali metals has been studied in some detail [1–14], in part to support the development of atomic frequency standards [15]. The pioneering work by Wood [1] on sodium has firmly established the importance of steady-state fluorescence techniques in studying quantum-resolved energy transfer [16]. The rates for energy transfer in rubidium induced by collisions with rare-gas atoms was examined by Beahn, Condell, and Mandelberg using resonance fluorescence techniques [4]. Krause [2] and Gallagher [3] continued this work improving the measurement of the cross sections and examining their temperature dependence. Further work using alkali-metal atoms as collision partners was performed by Vadla, Knezovic, and Movre, who measured the energy transfer cross sections for K and Cs [5]. Molecular collision partners, N_2, O_2, H_2, HD, D_2, H_2O, CH_4, CD_4, CH_2D_2, C_2H_4, and C_2H_6, have also been studied [6–13].

The importance of energy defect in these processes has been noted, particularly with regard to the variation in energy of the $n\,^2P_J$ levels for the alkali metals [2,3]. In the present paper we seek to measure the energy-transfer cross sections between the $5\,^2P_{3/2}$ and the $5\,^2P_{1/2}$ levels in rubidium caused by collisions with the molecular partners H_2, D_2, N_2, CH_4, and CF_4. In doing so, several discrepancies in the kinetic data base are resolved. The results are interpreted in terms of an electronic-to-rotational energy-transfer mechanism and the role of energy defect is examined. This work forms the basis for a detailed study of energy transfer between the Zeeman split levels of Rb($5\,^2P_{1/2,3/2}$), which is in progress [17].

II. EXPERIMENTAL DETAILS

The experimental apparatus for measuring the fine-structure mixing cross sections is depicted schematically in Fig. 1. A Coherent 899 Ti:sapphire ring laser provided up to 1.5 W near $\lambda=780$ or 794 nm to pump either the $^2S_{1/2}$-$^2P_{3/2}$ or the $^2S_{1/2}$-$^2P_{1/2}$ transition, as shown in Fig. 2. Side fluorescence as a function of laser power indicated a saturation intensity of 5.4 ± 0.6 mW/cm^2 and therefore the laser power was limited to 0.03 mW for a 0.2 cm beam diameter throughout the energy-transfer experiments. The ring laser linewidth is ≈0.5 MHz and laser excitation spectra indicate sufficient spectral isolation to pump from a single hyperfine component of the ground state for a single isotope [18]. Laser excitation of ^{87}Rb on the transitions $^2S_{1/2}(F=2)\rightarrow{}^2P_{1/2}(F=2)$ at $\lambda=794.70$ nm and $^2S_{1/2}(F=2)\rightarrow{}^2P_{3/2}(F=2)$ at $\lambda=780.02$ nm were used to prepare the $^2P_{1/2}$ and $^2P_{3/2}$ levels.

The rubidium cell has been described in detail previously [18]. To avoid photon trapping, the rubidium concentration was maintained at $\sim10^{-7}$ Torr.

The total side fluorescence from the rubidium sample cell was coupled into a bifurcated 8 mm core diameter incoherent fiber optic bundle, transmitted through two narrow-band interference filters, and detected using two thermoelectrically cooled RCA C31034 photomultiplier tubes (PMTs) via a photon counting system [17]. The interference filters limited detection to fluorescence primarily from either the D_1 line [$\lambda=795.1$ nm with a full width at half maximum (FWHM) of 1.2 nm] or the D_2 line ($\lambda=780.2$ nm with a FWHM of 1.2 nm). In this way, the emission from the laser pumped state, or parent state, and the emission from the collisionally populated, or satellite, state could be simultaneously and continuously monitored as a function of buffer gas pressure.

The windows of the fluorescence cell produced scattered

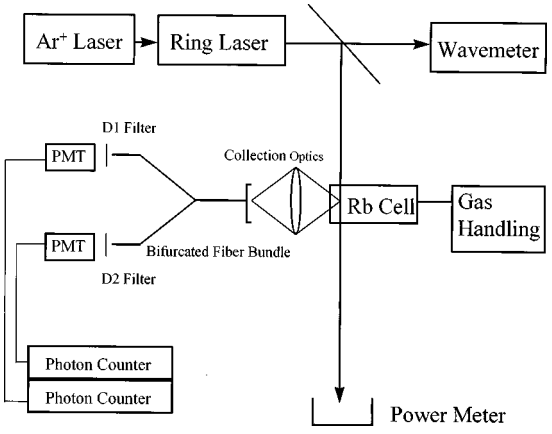

FIG. 1. Experimental apparatus for measuring the collisional energy-transfer cross sections between the $5\,^2P$ fine-structure split levels in rubidium.

*Present address: Phillips Laboratory/LIDB, 3550 Aberdeen SE, Kirtland AFB, NM 87117-5776.

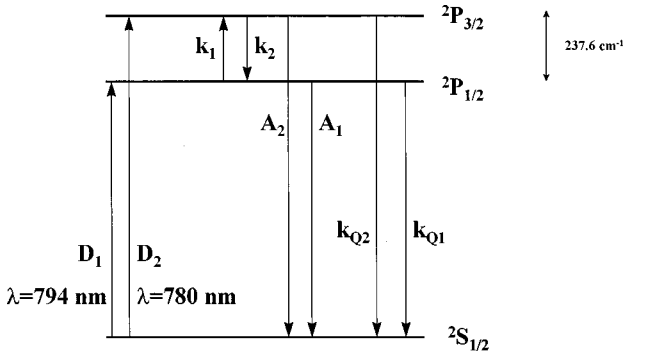

FIG. 2. Energy-level diagram for rubidium indicating kinetic processes.

laser light and, despite spatial filtering, were partially coupled into the fluorescence detection system. The intensity of this scattered laser light could be assessed by tuning the laser slightly off resonance of either the D_1 or D_2 absorption feature. Typically, 10–15 % of the emission on the parent line was due to scattered laser light, and was subtracted from the observed signal.

Unfortunately, the interference filters did not provide complete spectral isolation between the D_1 and D_2 lines, with about 2% of the intensity from the parent line being detected at the satellite wavelength. With no added buffer gas there is essentially no collisional transfer between the fine-structure states, and the fraction of the emission from the parent line observed at the satellite wavelength was directly observed. The satellite intensity was corrected at each buffer gas pressure by subtraction of this fraction of the parent signal at the same buffer gas pressure.

The intensity recorded at the two PMTs, corrected for laser scatter and filter leakage, is linearly related to the population of the emitting states:

$$I_{\lambda=794\ \mathrm{nm}} = d_1[\mathrm{Rb}\ (^2P_{1/2})], \tag{1}$$

$$I_{\lambda=780\ \mathrm{nm}} = d_2[\mathrm{Rb}\ (^2P_{3/2})], \tag{2}$$

where $I_{\lambda=794\ \mathrm{nm}}$ is the corrected signal from PMT filtered for D_1, $I_{\lambda=780\ \mathrm{nm}}$ is the corrected signal from PMT filtered for D_2, $[\mathrm{Rb}\ (^2P_{1/2})]$ is the concentration of $\mathrm{Rb}(^2P_{1/2})$, $[\mathrm{Rb}\ (^2P_{3/2})]$ is the concentration of $\mathrm{Rb}(^2P_{3/2})$, d_1 is the detectivity for emission from $\mathrm{Rb}(^2P_{1/2})$ through D_1 filter, and d_2 is the detectivity for emission from $\mathrm{Rb}(^2P_{3/2})$ through D_2 filter.

The detectivities d_i depend on radiometric factors, detector gains, filter and fiber transmissions, the spontaneous emission rates $A(^2P_{1/2}\text{-}^2S_{1/2}) = 3.70\times10^7\ \mathrm{s}^{-1}$ and $A(^2P_{3/2}\text{-}^2S_{1/2}) = 3.56\times10^7\ \mathrm{s}^{-1}$ [19], and a frequency factor of ν^3. The relative detectivities for emission from the two fine-structure states, $d_2/d_1 = 0.88\pm0.05$, were determined using a calibrated lamp source, and more precisely specified by requiring the resulting rates to obey the principle of detailed balance, as discussed below.

III. RESULTS

Typical data for the intensity observed from the satellite and parent emissions after laser excitation of $\mathrm{Rb}(^2P_{3/2})$ as a function of nitrogen buffer gas pressure is shown in Fig. 3. To obtain rate coefficients for energy transfer between the two spin-orbit split states from the observed intensities, a steady-state analysis of the kinetic mechanism as indicated schematically in Fig. 2 is required. Laser excitation selectively populates either the $^2P_{1/2}$ or $^2P_{3/2}$ states via the D_1 or D_2 transitions:

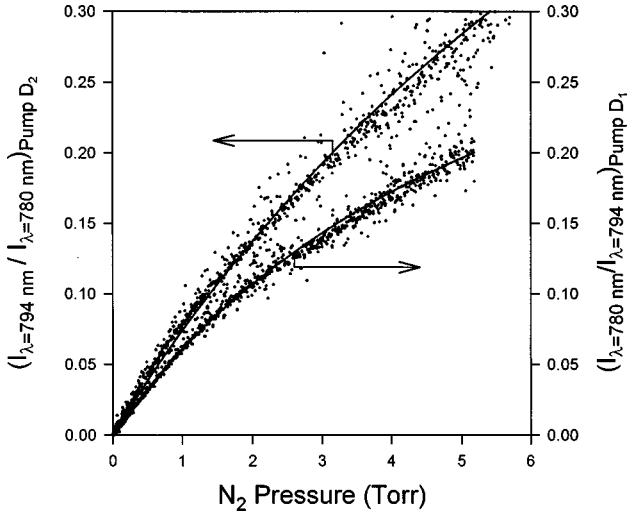

FIG. 3. Typical spin-orbit energy-transfer data in rubidium induced by N_2. The solid lines indicate fits to Eqs. (13) and (14).

$$\mathrm{Rb}(^2S_{1/2}) + h\nu \rightarrow \begin{cases} \mathrm{Rb}(^2P_{1/2}) & (\text{pump } D_1 \text{ at } \lambda=794\ \text{nm}) \quad (3) \\ \mathrm{Rb}(^2P_{3/2}) & (\text{pump } D_2 \text{ at } \lambda=780\ \text{nm}). \quad (4) \end{cases}$$

The energy transfer between spin-orbit split states, with rate coefficients k_1 and k_2, via collisions with buffer gas M is the primary process of interest:

$$\mathrm{Rb}(^2P_{1/2}) + M \rightarrow \mathrm{Rb}(^2P_{3/2}) + M, \tag{5}$$

$$\mathrm{Rb}(^2P_{3/2}) + M \rightarrow \mathrm{Rb}(^2P_{1/2}) + M. \tag{6}$$

Finally, spontaneous emission, with rates A_1 and A_2,

$$\mathrm{Rb}(^2P_{1/2}) \rightarrow \mathrm{Rb}(^2S_{1/2}) + h\nu, \tag{7}$$

$$\mathrm{Rb}(^2P_{3/2}) \rightarrow \mathrm{Rb}(^2S_{1/2}) + h\nu, \tag{8}$$

and collisional quenching, with rates k_{Q1} and k_{Q2},

$$\mathrm{Rb}(^2P_{1/2}) + M \rightarrow \mathrm{Rb}(^2S_{1/2}) + M, \tag{9}$$

$$\mathrm{Rb}(^2P_{3/2}) + M \rightarrow \mathrm{Rb}(^2S_{1/2}) + M, \tag{10}$$

remove population from the $^2P_{1/2,3/2}$ manifold. Analyzing the resulting rate equations under steady-state excitation conditions, for the excitation of $\mathrm{Rb}(^2P_{3/2})$, yields

$$\frac{[\mathrm{Rb}(^2P_{1/2})]}{[\mathrm{Rb}(^2P_{3/2})]} = \frac{k_2[M]}{A_1 + (k_{Q1}+k_1)[M]} \tag{11}$$

and for excitation of $\mathrm{Rb}(^2P_{1/2})$, yields

TABLE I. Cross sections for energy transfer between the $^2P_{1/2}$ and $^2P_{3/2}$ levels of rubidium induced by molecular collisions.

Collision partner	σ_1 (10^{-16} cm^2)	σ_2 (10^{-16} cm^2)	T (K)	Reference
H_2	10.0 ± 1.2	13.9 ± 1.7	330	this work
H_2	7 ± 3		340	[10]
H_2	26 ± 13		1720	[10]
H_2	>50	>30	1720	[8]
H_2	11	15	340	[7]
D_2	21.4 ± 2.6	29.8 ± 3.6	330	this work
D_2	22	30	340	[7]
N_2	13.2 ± 1.6	18.4 ± 2.2	330	this work
N_2	10 ± 5		340	[10]
N_2	20 ± 10		1720	[10]
N_2	99 ± 20	60 ± 12	1720	[8]
N_2	16	23	340	[7]
N_2	<2	7	300	[6]
O_2	66 ± 33	40 ± 20	1720	[8]
HD	18	25	340	[7]
H_2O	120 ± 25	73 ± 15	1720	[8]
CH_4	29.5 ± 3.5	41.0 ± 5.0	330	this work
CH_4		36	340	[9]
CH_4	30	42	340	[7]
CF_4	9.5 ± 1.1	13.2 ± 1.6	330	this work
CD_4		36	340	[9]
CD_4	28	38	340	[7]
CH_2D_2		37	340	[9]
C_2H_4	23	32	340	[7]
C_2H_6	57	77	340	[7]

$$\frac{[\mathrm{Rb}(^2P_{3/2})]}{[\mathrm{Rb}(^2P_{1/2})]}=\frac{k_1[M]}{A_2+(k_{Q2}+k_2)[M]}. \tag{12}$$

Thus the observed intensities are related to the buffer gas concentration via

$$\left(\frac{I_{\lambda=794\ \mathrm{nm}}}{I_{\lambda=780\ \mathrm{nm}}}\right)_{\mathrm{pump\ D_2}}=\left(\frac{d_1}{d_2}\right)\frac{k_2[M]}{A_1+(k_{Q1}+k_1)[M]} \tag{13}$$

and

$$\left(\frac{I_{\lambda=780\ \mathrm{nm}}}{I_{\lambda=794\ \mathrm{nm}}}\right)_{\mathrm{pump\ D_2}}=\left(\frac{d_2}{d_1}\right)\frac{k_1[M]}{A_2+(k_{Q2}+k_2)[M]}. \tag{14}$$

Figure 3 shows a fit of the observed intensities to Eqs. (13) and (14) yielding the fit parameters $(d_1/d_2)k_2$ and $(k_{Q1}+k_1)$ for excitation on the D_2 line and $(d_2/d_1)k_1$ and $(k_{Q2}+k_2)$ for the D_1 line. The values for the spontaneous emission rates, A_1 and A_2, were constrained to the values given above. A summary of the resulting collision cross sections, $\sigma_1=k_1/g$ and $\sigma_2=k_2/g$ where $g=\sqrt{8kT/\pi\mu}$ is the average relative speed, is provided in Table I. The curvature exhibited in the data of Fig. 3 is described by the removal rates in the denominators of Eqs. (13) and (14). This curvature is largely accounted for by the fine-structure transfer rates, k_1 or k_2, and an accurate determination of the quenching rate coefficients is not possible.

Note that the rate coefficients for energy transfer between the $^2P_{1/2}$ and $^2P_{3/2}$ levels must obey the principle of detailed balance [4]:

$$\frac{k_1}{k_2}=\frac{g_{J=3/2}}{g_{J=1/2}}\,e^{-\Delta E/kT}=0.72, \tag{15}$$

where the degeneracy $g_J=2J+1$ and $\Delta E=E(^2P_{3/2})-E(^2P_{1/2})=237.6\ \mathrm{cm}^{-1}$. Constraining the fit parameters via Eq. (15) provides the relative detectivities $d_2/d_1=0.88\pm0.05$ and the rate coefficients reported in Table I.

The largest source of error in the energy-transfer cross sections is from the uncertainty in the scattered laser light correction. The analysis of this correction results in a 12% uncertainty in the cross sections which is considerably larger than the statistical error obtained from the curve fit to the data.

IV. DISCUSSION

Rates for energy transfer are often greatest for mechanisms involving near-resonant excitation of the collision partner [16]. For example, the rates for energy transfer between the $^2P_{1/2,3/2}$ states of the atomic halogens are strongly correlated with the degree of energy match with $\Delta v=1,2$ vibrational transitions in the collision partner [19,20]. The energy separation between the $^2P_{1/2,3/2}$ states in the alkali metals is considerably less, from $17\ \mathrm{cm}^{-1}$ for Na to $237.6\ \mathrm{cm}^{-1}$ for Rb, and rotational excitation of the molecular collision partner is likely. The influence of rotational energy on the Rb-H_2 and D_2 fine structure changing collisions has been examined, and processes such as

$$\mathrm{Rb}(^2P_{3/2})+\mathrm{D_2}(J=0)\rightarrow\mathrm{Rb}(^2P_{1/2})+\mathrm{D_2}(J=2) \tag{16}$$

have been suggested to explain the large observed cross sections [10,11]. The $\Delta J=2$ transition in deuterium leads to a small energy defect, $\Delta E=-60\ \mathrm{cm}^{-1}$.

In an attempt to correlate the rate coefficients observed in the present and previous studies with energy defect for rotational transfer, we present the following simple model. Consider a more general form of reaction (16):

$$\mathrm{Rb}(^2P_{3/2})+M(J)\rightarrow\mathrm{Rb}(^2P_{1/2})+M(J+2), \tag{17}$$

where $M(J)$ represents an arbitrary molecular collision partner in rotational state J. Rotational excitation is limited to $\Delta J=2$ for simplicity and parity conservation [21,22]. The J-specific rate coefficients for reaction (17):

$$k(J)=A\ \exp(-|\Delta E|/kT) \tag{18}$$

are assumed to depend exponentially on the size of the energy defect:

$$\Delta E=[E(^2P_{1/2})-E(^2P_{3/2})]-[E_{\mathrm{rot}}(J+2)-E_{\mathrm{rot}}(J)], \tag{19}$$

where $E(^2P_{1/2})-E(^2P_{3/2})=237.6\ \mathrm{cm}^{-1}$ for rubidium, $E_{\mathrm{rot}}=B_vJ(J+1)$, and B_v is the rotational constant for the molecular collision partner M. For a statistical distribution among rotational levels, with partitioning $f(J)$, the average fine-structure rate coefficient would be

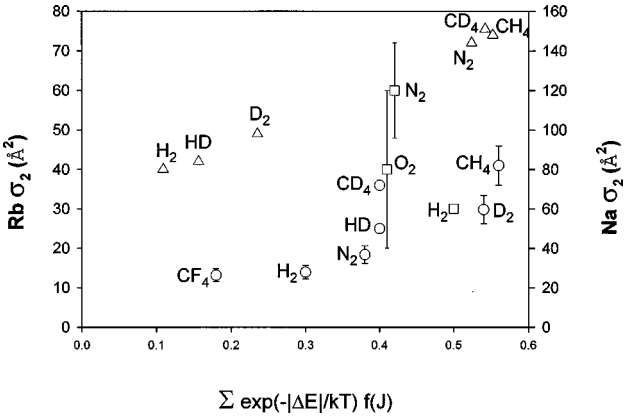

FIG. 4. Correlation of observed cross sections for fine-structure mixing of reaction (6) with the rotational-energy defect model of Eq. (20). Data for Na (△) from Refs. [23,24], for Rb (○) at $T=330-340$ K from present and previous [7,9] work, and for Rb (□) at $T=1720$ K from previous work [8].

$$k_{E\text{-}R}=\sum_J k(J)f(J)=\sum_J Ae^{-|\Delta E|/kT}\left(\frac{hcB_\nu}{kT}\right)\times(2J+1)e^{hcB_\nu J(J+1)/kT}. \quad (20)$$

A plot of the fine structure mixing rate coefficients for Rb and Na with molecular collision partners is shown as a function of the average rate coefficient $k_{E\text{-}R}$ in Fig. 4. The correlation is particularly good, considering the neglect of transition matrix elements in this analysis. It thus appears plausible that rotational energy of the molecular collision partner and electronic-to-rotational energy transfer plays an important role in the relaxation kinetics of the $^2P_{1/2,3/2}$ states in the alkali metals upon collision with molecular species.

V. CONCLUSIONS

Collisional mixing of the Rb $^2P_{1/2,3/2}$ states upon collision with molecular collision partners has been examined using steady-state laser-induced fluorescence techniques, which provide continuous monitoring of the populations as a function of buffer gas pressure and improved accuracy in the reported rate coefficients. The transfer cross sections for Rb and Na are strongly correlated with rotational energy defect, suggesting an electronic-to-rotational energy-transfer mechanism.

ACKNOWLEDGMENT

This work was supported in part by a grant from the Air Force Office of Scientific Research.

[1] R. W. Wood, Philos. Mag. **27**, 1018 (1914).
[2] L. Krause, Appl. Opt. **5**, 1375 (1966).
[3] A. Gallagher, Phys. Rev. **172**, 88 (1968).
[4] T. J. Beahn, W. J. Condell, and H. I. Mandelberg, Phys. Rev. **141**, 83 (1966).
[5] C. Vadla, S. Knezovic, and M. Movre, J. Phys. B **25**, 1337 (1992).
[6] J. A. Bellisio, P. Davidovits, and P. J. Kindlmann, J. Chem. Phys. **48**, 2376 (1968).
[7] E. S. Hrycyshyn and L. Krause, Can. J. Phys. **48**, 2761 (1970).
[8] P. L. Lijnse, P. J. Th. Zeegers, and C. Th. J. Alkemade, J. Quant. Spectrosc. Radiat. Transf. **13**, 1033 (1973).
[9] R. A. Phaneuf and L. Krause, Can. J. Phys. **58**, 1047 (1980).
[10] J. M. Mestdagh, P. de Pujo, J. Cuvellier, A. Binet, P. R. Fournier, and J. Berlande, J. Phys. B **15**, 663 (1982).
[11] J. Cuevellier, J. M. Mestdagh, M. Ferray, and P. de Pujo, J. Chem. Phys. **79**, 2848 (1983).
[12] A. P. Hockman, J. Phys. B **15**, 3005 (1982).
[13] J. Pascale, F. Rossi, and W. E. Baylis, Phys. Rev. A **36**, 4219 (1987).
[14] E. E. Nikitin, J. Chem. Phys. **43**, 744 (1965).
[15] R. E. Olson, Chem. Phys. Lett. **33**, 250 (1975).
[16] J. T. Yardley, *Introduction to Molecular Energy Transfer* (Academic, New York, 1980).
[17] M. D. Rotondaro, *Collisional Dynamics of the Rubidium 5^2P Levels* (University Microfilms International, Ann Arbor, MI, 1995).
[18] M. D. Rotondaro and G. P. Perram, J. Quant. Spectrosc. Radiat. Transf. **57**, 497 (1997).
[19] J. K. Link, J. Opt. Soc. Am. **56**, 1195 (1966).
[20] P. L. Houston, Adv. Chem. Phys. **47**, 381 (1981).
[21] C. W. McCurdy and W. H. Miller, J. Chem. Phys. **67**, 463 (1977).
[22] G. P. Perram, D. A. Massman, and S. J. Davis, J. Chem. Phys. **99**, 6634 (1993).
[23] M. Stupavsky and L. Krause, Can. J. Phys. **46**, 2127 (1968).
[24] M. Stupavsky and L. Krause, Can. J. Phys. **47**, 1249 (1969).